When and why the Neo-Tethyan subduction initiated along the Eurasian margin: a case study from a Jurassic eclogite in southern Iran

Bo Wan [a]*, Yang Chu[a], Ling Chen[a], Zhiyong Zhang[a], Songjian Ao[a], Morteza Talebian[b]

[a] *State Key Laboratory of Lithospheric Evolution, Institute of Geology and Geophysics, Chinese Academy of Sciences, Beijing 100029, China*

[b] *Research Institute for Earth Sciences, Geological Survey of Iran, Azadi Square, Meraj Blvd, Tehran, Iran*

Accepted July 18 2022

Chapter in AGU book titled as "Tectonics Processes: a Global View" Volume II "Compressional Tectonics: Plate Convergence to Mountain Building" edited by Elizabeth Catlos and Ibrahim Çemen

* Corresponding author. E-mail: wanbo@mail.iggcas.ac.cn;

Tel: +86-10-8299-8154; Fax: +86-10-6201-0846

Abstract

Tethyan evolution is characterized by cyclical continent-transfer from Gondwana to the continents in the Northern Hemisphere, similar to a “one-way” train. Subduction has been viewed as the primary driver of transference. Therefore, it is crucial to understand the tectonic evolution of all past subduction zones that occurred along Eurasia's southern margin. We studied the earliest known eclogite located at the Neo-Tethyan suture in the Iranian segment. A prograde-E-MORB-like eclogite reached a peak metamorphic condition of 2.2 GPa and 560°C, at 190 ± 11 Ma (1σ rutile U-Pb ages), which constrains the youngest age for subduction initiation of the Neo-Tethyan slab. Combined with regional magmatic and structural data, the oldest age for Neo-Tethys subduction initiation is 210–192 Ma, which is younger than the Paleo-Tethyan closure time of 228–209 Ma. These data, used with previous numerical modeling, supports collision-induced subduction initiation. The collision-induced force, together with the Paleo-Tethyan subduction driven-mantle flow, is likely to have exploited weak inherited structures from earlier Neo-Tethyan rifting, resulting in a northward directed subduction zone along the southern margin of Central Iran Block.

Key words: continental rifting, collision-induced, subduction initiation, Neo-Tethyan, Tethyan dynamics

1. Introduction

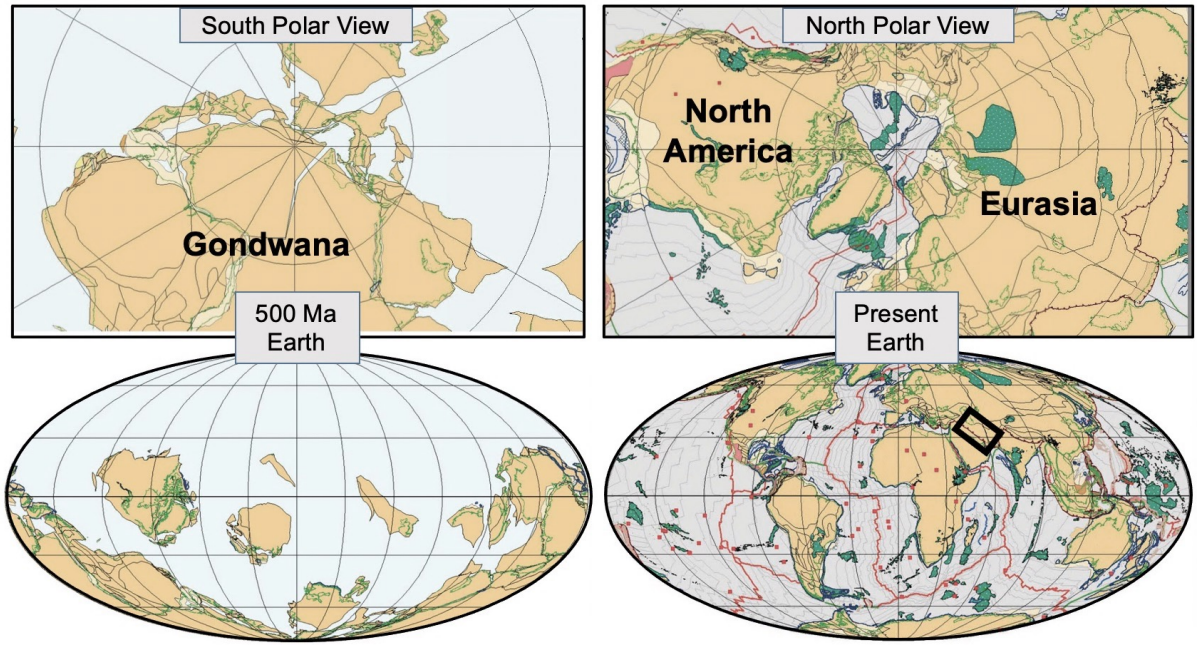

Figure 1. Views of Earth. Left: the South Polar view of the Earth and world map (at 500 Ma); Right: the North Polar map of the Earth and world map (present day) adapted from Lawver et al. (2015). Light grey: continent; dark grey: large igneous provinces. The study area is denoted by a black square.

Currently, with the exception of Antarctica, most continents are connected and encircle the north pole (Fig. 1). Almost all continents, including Gondwana, were located in the central to southern hemisphere to cap the south pole at about 500 Ma (Lawver et al., 2015). The one-way mega-transferring of continents from south to north was a key event of Earth, that occurred during the last 500 million years (Myr), with the Australian continent moving north at a rate of 70 mm/year as a representative active example (DeMets et al., 2010). During this mega-transferring of continents, the sea-land paleogeography changed, which influenced the Earth's surface temperature from an icy to a warmer world (Merdith et al., 2019; Bergman et al., 2021; Scotese et al., 2021). However, the driving mechanism for this one-

61 way/single-directed transfer is still debated. Two competing theories are: (1) whole
62 mantle convection which involves plume upwelling and subduction (e.g. Becker and
63 Faccenna, 2011; Jolivet et al., 2016; Faccenna et al., 2021); and (2) northward
64 oceanic subduction (Wan et al., 2019; Wu et al., 2020). After 50 Ma, the Indo-
65 Australian oceanic plate began subducting beneath the southern Eurasian continent
66 (Sunda Shelf) margin along the Java trench (Hall, 2017). The major eruption of the
67 Kerguelen large igneous province (90–120 Ma) has been proposed to have
68 fragmented the Antarctic-Australia plate. However, this eruption was earlier than the
69 abrupt velocity change of the Australia plate at 45 Ma (Whittaker et al., 2013;
70 Williams et al., 2019). Instead, the Australian plate acceleration is temporally closer
71 with that of the 50 Ma Java trench subduction zone activity. This supports the idea
72 that subduction is the driving force of the northward migration of the Australian plate
73 (Forsyth and Uyeda, 1975).

74 The cycle of Tethyan oceans involved the Proto-Tethys (440–420 Ma closure),
75 the Paleo-Tethys (330–220 Ma closure), and the Neo-Tethys (65–15 Ma closure).
76 This cycle merged many Gondwana-derived continents with continents to the north.
77 All surviving Tethyan sutures are presently located in the northern hemisphere
78 (Stampfli et al., 2013; Torsvik and Cocks, 2017; Wu et al., 2020). It is unclear if the
79 closure of the Tethyan oceans was caused by the same tectonic forces that are
80 controlling the current evolution of the Indian Ocean and the northward migration of
81 the Australian plate. To compare these two scenarios, it is necessary to first
82 constrain the subduction initiation for the Tethyan oceans, in particular the youngest

Neo-Tethyan ocean. However, subduction initiation is a challenging and poorly understood topic (Stern and Gerya, 2018), especially given the discrepancy between numerical modeling (Gerya et al., 2015; Leng and Gurnis, 2015; Zhong and Li, 2020; Zhou et al., 2020; Zhong and Li, 2022), and geological observations (Whattam and Stern, 2011; Guilmette et al., 2018; van Hinsbergen et al., 2021).

The Neo-Tethyan Iranian segment preserves many Neo-Tethyan ophiolites (Moghadam and Stern, 2015; Ao et al., 2016), subduction-related magmatic episodes (Omrani et al., 2008; Chiu et al., 2013; Chiu et al., 2017; Zhang et al., 2018; Moghadam et al., 2022), and metamorphic events (Agard et al., 2011; Davoudian et al., 2016; Bonnet et al., 2020). This makes the Iranian segment an ideal location to study the Neo-Tethyan subduction initiation problem. There is a consensus about Neo-Tethyan subduction initiation along the southern Iranian continent's margin (Hassanzadeh and Wernicke, 2016; Stern et al., 2021). However, the timing of Neo-Tethyan subduction initiation in Iran is debated, and either occurred in the Triassic-Jurassic (Arvin et al., 2007), or the Cretaceous (Moghadam and Stern, 2015). In addition, the driving mechanism has been explained through either collision-induced (Wan et al., 2019), or spontaneous nucleation (Moghadam and Stern, 2011) Additionally, it is crucial to understand why the subduction of the Indian, Neo-Tethyan, and Paleo-Tethyan ocean basins consistently initiate along the southern Eurasian margin with a north-dipping slab, as opposed to how subduction polarity frequently reverses in the southern hemisphere in the Pacific realm (Brown and Ryan, 2011).

Figure 2: Tectonic sketch map of Iran, highlighting tectonic domains, Neo-Tethyan suture, Jurassic magmatism, and high-pressure metamorphism. Based on the map from the Geological-Survey-of-Iran (2009). Strata observation positions from Leven and Gorgij, (2011).

In this study, an eclogite sample along the Neo-Tethyan suture zone in southern Iran was analyzed to find out its photolith nature, in situ metamorphic age, and its corresponding metamorphic condition based on geochemical-petrological studies. The new in-situ U-Pb rutile age is the earliest subduction-related high-pressure metamorphic event observed in the Neo-Tethyan suture zone. This event defines the latest (youngest) timing of subduction initiation. In addition, the mechanism for how

and why subduction occurred is discussed with the goal to better understand other Tethyan regions and subduction zones globally.

2. Geological background

Three major tectonic domains dominate the Tethyan evolution in Iran. Along the Talesh-Alborz-Binalud mountain range in northern Iran, the Paleo-Tethyan suture divides the Kopeh-Dagh domain to the north from the Central Iran domain to the south. The Neo-Tethyan closure sutured the Central Iran domain and Arabia domain in southern Iran. The Kopeh-Dagh is dominated by Jurassic to Cenozoic shallow marine to continental sedimentary rocks such as: limestone, sandstone, shale, and conglomerate. The basement of the Kopeh-Dagh domain is a Paleozoic–Early Mesozoic volcanic arc located on the Baltic or Siberian Precambrian continents (Natal'in and Şengör, 2005; Zanchetta et al., 2013; Chu et al., 2021).

According to sedimentary records, the entire central Iran domain was formerly part of the Arabian continent but separated as a ribbon continent (Cimmeria) in the late Permian (Koop et al., 1982). During the rifting and drifting process, Central Iran was surrounded by passive margins, as indicated by sedimentary facies analyses (Leven and Gorgij, 2011), which share a similar scenario of Indian drifting northward during the Cretaceous. Recent research in northern Iran, along the Paleo-Tethyan suture near Mashhad, indicate that the first arrival of Eurasian material to the passive margin of central Iran occurred at 209–228 Ma (Chu et al., 2021). Previous stratigraphic studies suggest that the collision must have occurred between the late

Triassic (228 Ma) and the mid Jurassic (174 Ma), and possibly initiated at the Carnian–Norian boundary (Fürsich et al., 2009). Additionally, the extensive time span might be restricted by a stitching pluton at 217 ± 1.7 Ma (2σ) that crosscuts through Triassic compressional structures in the Alborz (Zanchetta et al., 2013). Thus, the new detrital zircon results (209–228 Ma) (Chu et al., 2021), corroborate prior stratigraphic and structural geological studies (217–228 Ma), implying a Triassic collision event.

Magmatism is extensive in Central Iran, with two magmatic flare-ups occurring in the Jurassic along southern Iran (Fig. 2), and in the Cenozoic throughout Central Iran (Verdel et al., 2011; Chiu et al., 2013; Zhang et al., 2018; Moghadam et al., 2022). The Jurassic plutons are mostly granite, granodiorite, quartz diorite, and gabbro (Hassanzadeh and Wernicke, 2016), whilst the Jurassic volcanic rocks are mostly basaltic, andesitic lava, and volcanoclastics (Emami and Khalili, 2008). Geochemical studies on the Jurassic igneous rocks found $\varepsilon Hf_{(T)}$ values ranging from +13 to −3 (Chiu et al., 2017; Zhang et al., 2018), indicating that they originated from a mixed juvenile and reworked crustal sources. The Hf isotopic ratios of Jurassic igneous rocks are in the range of Cenozoic igneous rocks $\varepsilon Hf_{(T)}$ (+14 to -7) along southern Iran (Chiu et al., 2017; Moghadam et al., 2022). The similar petrological and geochemical features between Jurassic and Cenozoic magmatic rocks implies a similar subduction-related tectonic environment, while some researchers think that the Jurassic rocks have inherited the geochemical signature from a Mesozoic continental rifting episode (Azizi and Stern, 2019).

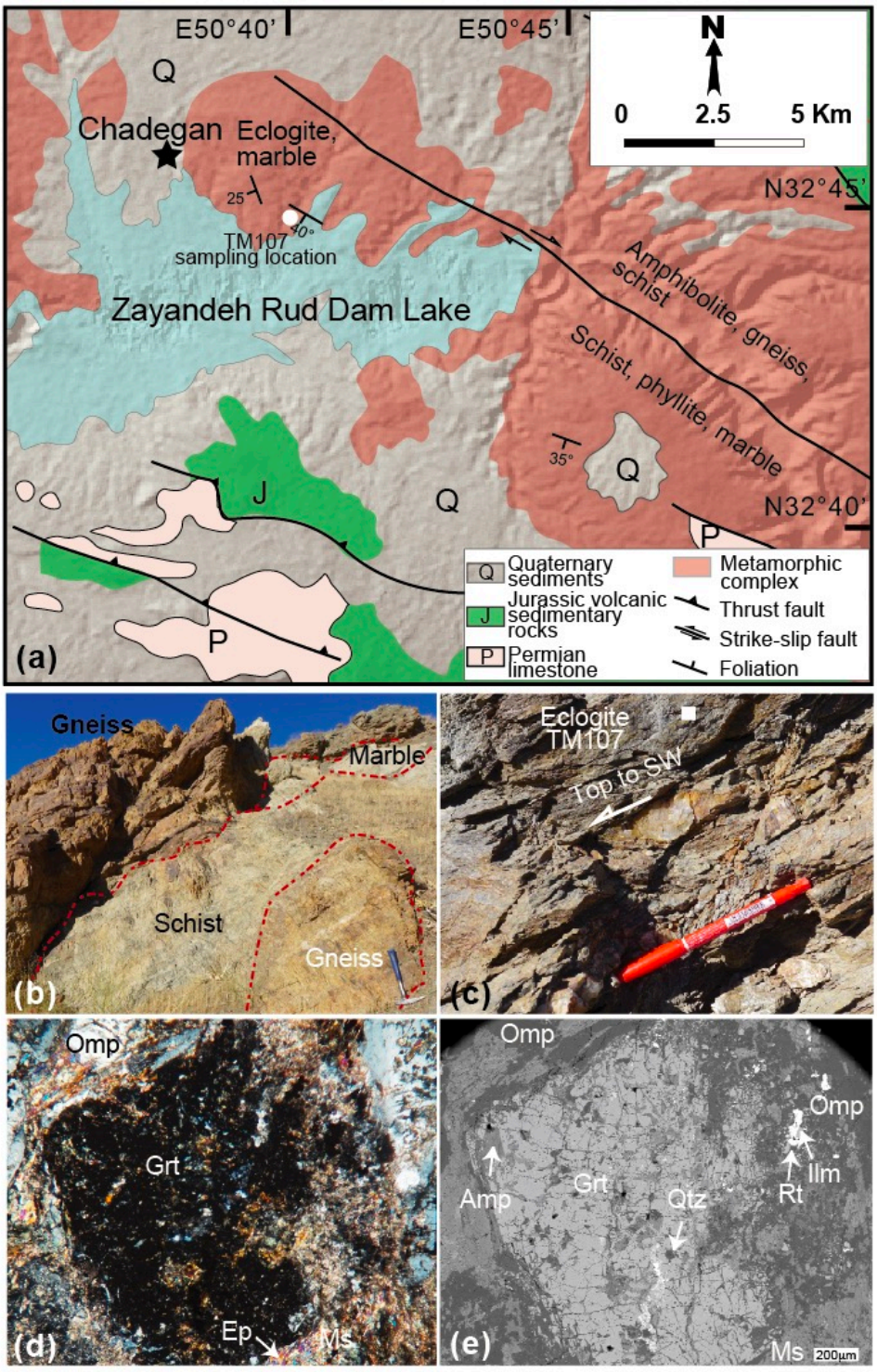

Figure 3. (a) Simplified geological map showing the juxtaposition of various rock types and metamorphic grades of rocks, based on the Shahrekord Sheet of the Geological-Survey-of-Iran (2009). (b) Marble lenses in schist and gneiss. (c) Top-to-the-SW fabric in eclogite (white square marks the thin section site). Two thin section photos (d: cross polarized light, e: backscattered electron)

showing the major mineral associations. Grt: garnet, Omp: omphacite, Rt: rutile, Amp: amphobile, Qtz: quartz, Ilm: ilimnite, ep: epidote, and Ms: mica

Along southern Iran, Jurassic high-pressure low-temperature (HP/LT) metamorphic rocks have been reported (Davoudian et al., 2016; Jamali Ashtiani et al., 2020). The HP/LT rock is an eclogite with a peak metamorphic condition of 2.35–2.5 GPa and 520–600°C, and metamorphic ages of 172–184 Ma by Ar-Ar dating of phengite (Davoudian et al., 2016). The eclogites outcrop along a regional NW-striking shear zone (Fig. 3), and the field relationship has been described in detail by (Davoudian et al., 2016). Eclogite bodies and marbles occur as lenses in the schist, and the lenses are mostly meters-scale. The marble lenses contain dark eclogite, indicating the marble has also undergone HP metamorphism. The schist is at amphibolite-grade, with greenschist in the surrounding region. The ages of the schists are still unknown. Recent studies show that the gneisses are from Cadomian basement, with an age of 552 Ma, which also containing a younger intrusion dated as 176 ± 3.3 Ma (2σ) (Jamali Ashtiani et al., 2020). Permian limestone, Jurassic volcanic-sedimentary rocks are thrust over the metamorphic complex with various grades of metamorphic rocks such as schist, gneiss, and amphibolite. The Jurassic volcanic-sedimentary rocks have experienced low-grade metamorphism, at prehnite–pumpellyite facies. This type of rock assemblage, with different origin with contrasting metamorphic grades is very similar to the accretionary complex associated with subduction zones observed globally (Wakabayashi, 2011).

Additionally, understanding the origin of the HP/LT rocks will aid in comprehending the subduction environment at the time.

Many early Cretaceous ophiolites occur in the south of Central Iran (Moghadam and Stern, 2011; Moghadam and Stern, 2015), and extensive Cretaceous to Cenozoic magmatic rocks are viewed as the subduction products of the Neo-Tethyan slab (Omrani et al., 2008; Moghadam et al., 2022). The final closure of the Neo-Tethys merged the Central Iran domain with the Zagros domain along the Zagros suture during the Oligocene or the Miocene (McQuarrie and van Hinsbergen, 2013; Zhang et al., 2017).

3. Sample, analytical methods and results

In the Shahrekord region, we sampled an eclogite (TM107, N32°45'47" E50°39'37") near Chadegan (Fig. 3). The eclogite is composed of garnet, omphacite, muscovite, chlorite, barroisite, calcic-amphibole, epidote, quartz, rutile, and ilmenite. The metamorphic mineral assemblage at its peak is composed of amphibole, muscovite, garnet, omphacite, quartz, and rutile.

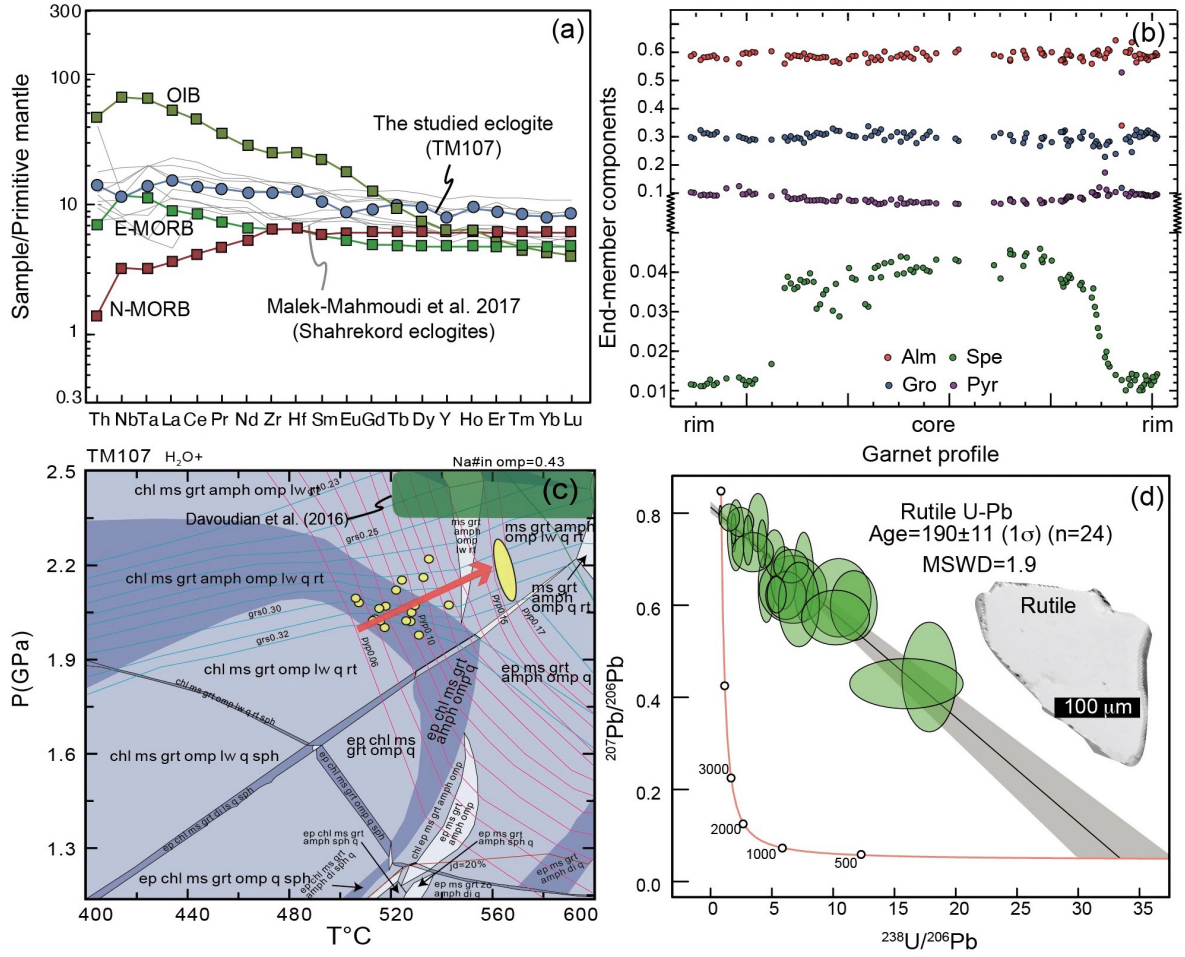

Figure 4. Analytical results from bulk sample or minerals from studied eclogite sample TM107. (a) Primitive mantle-normalized trace-element pattern, normalizing data from Sun and McDonough (1989). (b) EMPA profiles showing homogenous components of Mg, Ca, Al and decreasing Mn garnet end-member components from core to rim in garnet grain; (c). P–T pseudosection (SiO_2 48.23, TiO_2 1.89, Al_2O_3 14.51, FeO 12.86, MgO 7.54, CaO 11.18, Na_2O 2.62, MnO 0.24, K_2O 0.65 wt.%, which is corrected from table 1). Ellipse region is calculated from EPMA data of garnet (Supplementary table), and rectangle region from Davoudian et al. (2016). (d) Rutile SIMS U-Pb age.

The sample was ground the sample into 200-mesh powder and the bulk-sample's major and trace elements geochemistry was analyzed to determine the rock's origin. To understand the metamorphic processes and peak metamorphic

conditions, we chose a representative garnet was selected for major oxide measurements and P-T pseudosection modeling. Additionally, rutile was separated and the U-Pb isotopes were analyzed to determine the absolute age of peak metamorphism. Rutile was used as it formed at a peak metamorphic stage, is in equilibrium with garnet, and has an appropriate U-Pb system closure temperature of ~600°C, with a proper crystal size (Cherniak, 2000). The analyses were undertaken by various facilities at the Institute of Geology and Geophysics, Chinese Academy of Sciences. The details are described in the supplementary file.

The eclogite sample (TM107) has SiO_2 of (47.02 wt. %), Fe_2O_{3T} (13.92 wt. %), TiO2(1.84 wt. %), MgO (7.34 wt. %), Na_2O (2.55 wt. %), CaO (7.94 wt. %), K_2O (0.65 wt. %), and negligible P_2O_5. The eclogite is characterized by a slightly enriched light-rare-earth element pattern (La/Yb = 2.68). It shares a typical composition with that of enriched middle-ocean ridge basalt (E-MORB) (Sun and McDonough, 1989) (Fig. 4a; Table 1). The garnet is relatively homogenous with Fe and Al, belonging to the almandine end-member, and shows a decrease in Mn from the core to the rim along a profile across the mineral (Fig. 4b). The compositions of minerals and bulk-rock are presented in detail in Table 1 and Supplemental Table. The garnet-derived P-T conditions constrain a prograde path with a maximum P-T condition of 2.2 GPa and 560°C and a geothermal gradient of 7.7°C/km (Fig. 4c). Exhumation of the eclogite resulted in the production of epidote and amphibole following peak metamorphism. The modeling result agrees with the thin section observations, indicating that rutile formed at the garnet rim during peak metamorphism. A total of

32 rutile grains (each with a 100 μm crystal size) was measured for U-Pb isotopes, with 24 grains providing valid data (Table 2). The U concentration is modest (1.8–0.3 ppm), while the Th/U ratio varies between 0.01 and 0.33. The valid 24 analyses yield a lower intercept age of 190 ± 11 Ma (1σ) with an MSWD of 1.9., as shown on the Terra-Wasserburg diagram (Fig. 4d).

4. Discussion

4.1. Neo-Tethyan subduction initiation time

Most researchers agree that Neo-Tethyan subduction began at the southern margin of Central Iran, but disagree on the timing of initiation between the Triassic-Jurassic (Arvin et al., 2007; Ahadnejad et al., 2011; Chiu et al., 2013; Davoudian et al., 2016; Zhang et al., 2018) and the late Cretaceous (Moghadam and Stern, 2015). The widespread magmatism in the early Jurassic in Central Iran clearly shows arc signatures of depleted Hf isotopes (Chiu et al., 2017; Zhang et al., 2018), which are regarded as an upper constraint (earliest age) of subduction initiation. Some researchers attribute a late Triassic Siah-Kuh granite (200 ± 30 Ma (2σ) Sm-Nd isochron as the earliest evidence (Arvin et al., 2007). However, the updated LA-ICPMS zircon U-Pb dating gave ages of 175 ± 1.8 Ma (2σ) from the Siah-Kuh granite (Chiu et al., 2013), and now the earliest and most reliable arc magmatism in southern Iran is a 187 ± 6 Ma (2σ) granodiorite (Ahadnejad et al., 2011) (Fig. 2). Stern (2004) suggested that the age of the SSZ-type ophiolite could represent subduction initiation. The earliest SSZ-type ophiolites in southern Central Iran along

261 the Turkish-Zagros suture formed 90 ± 10 Ma (Whattam and Stern, 2011;
262 Moghadam and Stern, 2015), which is significantly younger than the Jurassic
263 subduction arc magmatism (Zhang et al., 2018).

264 In contrast, the oldest HP rocks associated with subduction in the accretionary
265 complex may provide better evidence for subduction initiation. Using the phengite Ar-
266 Ar technique, the earliest eclogite was dated as being 184 ± 1 Ma (1σ) (Davoudian et
267 al., 2016). The sub-arc depth is known to be 100 kilometers, which corresponds to
268 the location of the majority of arc magma production (Syracuse and Abers, 2006).
269 HP metamorphism in a subduction zone mostly occurs at a fore-arc depth that is
270 shallower than the sub-arc depth (Agard et al., 2009). As a result, the earliest HP
271 metamorphic age in the subduction zone should be older than the earliest magmatic
272 arc rock formed following subduction initiation (only if these rocks have been
273 preserved and discovered). The eclogite contains E-MORB geochemistry that is
274 consistent with a previous report by Malek-Mahmoudi et al. (2017), indicating an
275 oceanic slab subduction environment (Fig. 4). The in-situ rutile U-Pb dating method
276 yielded an age of 190 ± 11 Ma (1σ) with an MSWD of 1.9. This new in-situ rutile age
277 is slightly older than the oldest arc magmatism (187 Ma) in Central Iran. The Mn
278 concentration of garnet from the eclogite is enriched in the core and is depleted in
279 the rim, indicating that the eclogite was under prograde metamorphism (Fig. 4d).

280 This study calculates that the eclogites experienced a geothermal gradient of 7°–
281 7.7 °C/km, which replicates the results from Davoudian et al. (2016). These
282 temperatures are within typical subduction zone geothermal gradients of 5–10 °C/km

283 (Wang et al., 2021). However, numerous geological and numerical investigations
284 revealed a hot subduction environment during subduction initiation that is
285 characterized by high-temperature rocks such as boninite and a metamorphic sole
286 (Stern, 2004; Esna-Ashari et al., 2016; Maunder et al., 2020; Coulthard Jr et al.,
287 2021). While the new rutile U-Pb age from the eclogite sample constrains the oldest
288 subduction-related timing in the Iranian Neo-Tethyan region to date, it represents the
289 closest time lagged after the subduction initiation with respect to previous studies
290 (Ahadnejad et al., 2011; Davoudian et al., 2016). Unlike the records in Iran, Early
291 Jurassic ophiolites and accretionary complexes are well documented in Turkey, to
292 the west of Iran, along the strike (Topuz et al., 2013; Okay et al., 2020). The geology
293 in Turkey would help the correlation of the Jurassic subduction zone along the
294 southern Eurasian margin, in southern Iran with the nearby region.

295 Nikolaeva et al. (2010) modeling experiments suggest that the transition from a
296 stable margin to subduction initiation at a passive margin is controlled by the ductile
297 strength of the lower continental crust, subcontinental lithospheric mantle, and the
298 density contrast with the suboceanic lithospheric mantle. The modeled transition
299 takes 1 Myr to ~45 Myr to initiate subduction. However, new numerical modeling
300 examined the time of subduction initiation at passive margins, and determined that
301 subduction could occur only in the presence of a weak zone at the passive margin
302 Zhong and Li (2020). If a horizontal convergence force (larger than 3.0×10^{12} N/m)
303 is exerted on the passive margin, the transition duration from passive to subduction
304 is between ~2 Myr to ~20 Myr, but for most cases are less than 10 Myr (Zhong and

Li, 2020). As previously estimated, the subduction plate at 700 km depth would exert 4.9×10^{13} N/m force on the trench plate (Wan et al., 2021). Previous modeling shows that the net slab force to pull the trailing plate is 10% of the slab pull force (Schellart, 2004), ~ 4.9×10^{12} N/m for the Iranian Tethys case. After initial collision, and before slab breakoff, the net slab pull force together with the ridge push force from Neo-Tethyan mid-ocean should match the numerical modeling requirements of Zhong and Li (2020). The new rutile age of 190+11 Ma (1σ) from the geological observation is not conflict with the results from numerical tests in Zhong and Li (2020)(Fig. 5). The earliest subduction initiation at a passive margin should occur between 192 and 210 Ma.

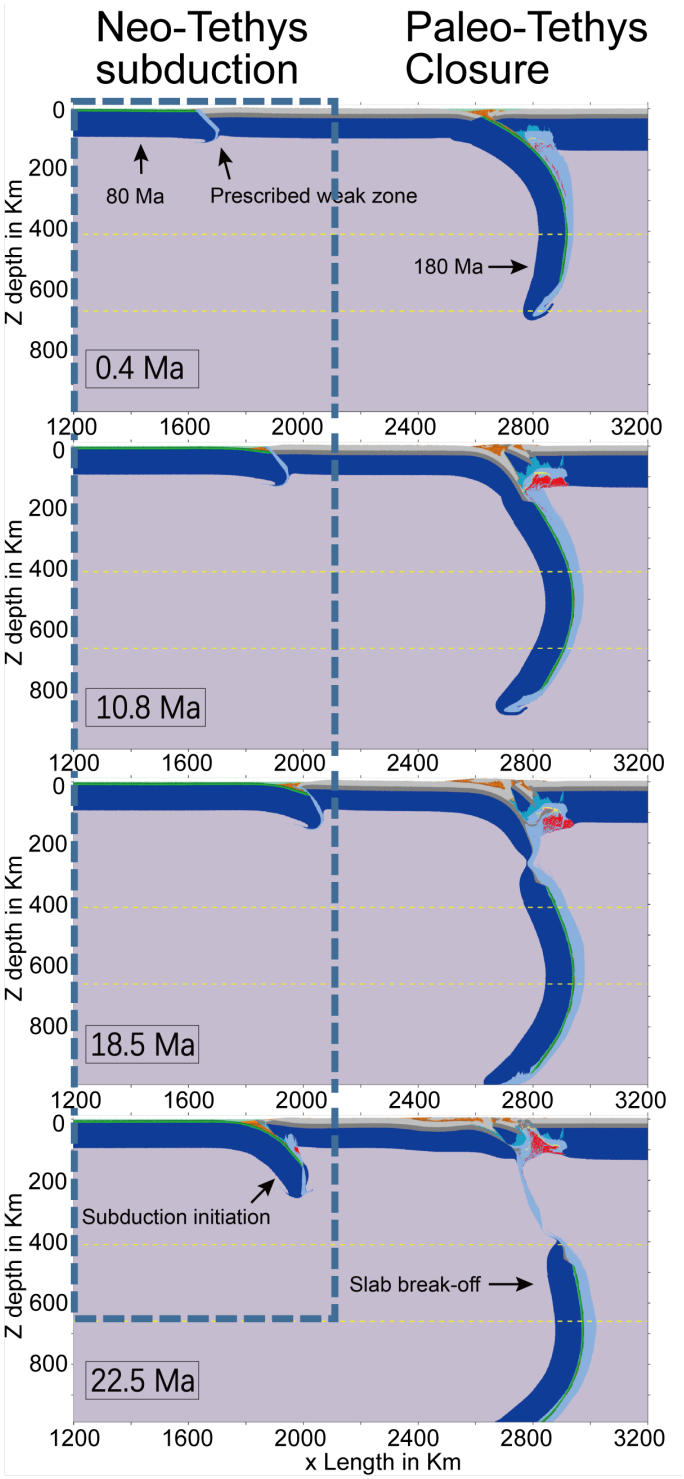

315

316 **Figure 5. Convergent boundary force of 3.0 × 10^{12} N/m, with a prescribed weak**
317 **zone at the passive margin model showing the subduction initiation taking**
318 **22.5 Myr after collision. Dashed boxes mark the passive margin. After**
319 **Zhong and Li (2020)**

320

4.2. Mechanism of Neo-Tethyan subduction initiation from the Eurasian margin

The boundary between the Neo-Tethyan oceanic plate and Central Iran continental crust is the location where the Neo-Tethyan subduction zone initiated. This is because no earlier oceanic island arc (older than 100–120 Ma) has been reported in the southern Central Iran (Moghadam and Stern, 2011; Moghadam and Stern, 2015). Central Iran has a current size of approximately 1 million km^2. Considering the shortening rate of Central Iran during the Arabian-Eurasian collision, including the older Cimmerian orogeny, its original size must be larger than its current size and could be comparable with the size of the Ontong Java oceanic plateau of 1.5 million km^2. Niu et al. (2003) showed that a plume-modified oceanic lithosphere is ~1% less dense than a normal oceanic lithosphere. According to new numerical modeling studies, an oceanic plateau with a strong rheological and depleted mantle root could assist the subduction zone by transferring from a plateau-continent collision zone to a plateau-oceanic boundary (Yan et al., 2021). Central Iran must be even lighter than an oceanic plateau because of the lighter continental lithosphere and thicker and lighter sedimentary cover. Therefore, its resistance to subduction during collision should be even more likely. To induce a new subduction zone, it is necessary to provide a continuous convergent force to overcome the lithospheric rigidity. The convergent force at the southern margin of Central Iran is controlled by the interplay between Central Iran and Eurasia colliding. The northward collision force is provided by the Paleo-Tethyan slab's northward subduction prior to

its separation from Central Iran and its lateral continents. According to van Hunen and Allen (2011) numerical modeling experiments, the older the oceanic crust is, the stronger it is and requires a longer period (over 20 Myr) to break-off. Because the Paleo-Tethyan opening occurred earlier than the Devonian (Chu et al., 2021), the late Triassic collision formed the subducting boundary between the Paleo-Tethyan slab and Central Iran. Such a prolonged time span indicates the presence of a strong oceanic lithosphere. As a result, the subducting Paleo-Tethyan slab may give at least another 20 Myr of convergence following collision. The docking/amalgamation and growth of mountains in northern Iran may have absorbed part of the horizontal convergence. However, kilometer-scale uplift cannot absorb all of the convergence from hundreds or even thousands of kilometers of continental collision. Following the ultimate break-off of the Paleo-Tethyan slab, the low density continental crust in the mantle will be exhumed to a shallow depth due to its buoyancy, providing an extra force to supply the southern Central Iran margin with the convergent force required to initiate subduction. Thus, following continental collision, several geological processes may generate horizontal convergence stresses sufficient to initiate subduction along pre-existing weak zones in the Gondwana lithosphere (Fig. 5d).

The newly constrained timing of collision at 228–209 Ma indicates that a continuous convergent force can continue to 208–189 Ma before slab break-off (van Hunen and Allen, 2011; Zhong and Li, 2020; Chu et al., 2021). This coincides with our new predicted Neo-Tethyan subduction initiation time range of 210–192 Ma. This study's limitation is that observation of geological events such as continental collision,

subduction initiation, and accompanying slab break-off, cannot be as precise as numerical modeling, and geological events may be diachronous along strike. However, the sequence between continental collision and subduction initiation remains constant. According to updated information, the Iranian Neo-Tethys subduction began between 210 and 192 Ma, which is younger than the final closure of the Paleo-Tethys in northern Iran, which occurred between 228 and 209 Ma (Fig. 6a). Similar scenarios occurred in other Tethyan regions, such as in Bulgaria, Turkey, Tibet, and southeast Asian regions (see Wan et al., 2019 and references therein), which may have broad implications for subduction zone transfer in Tethyan collision events.

The Neo-Tethyan region's continental collision-induced subduction initiation may be distinct from the Pacific region, as there are numerous cases of subduction polarity reversal in the south to west Pacific (Brown and Ryan, 2011). During the Tethyan development, the new subduction in the Neo-Tethys and Indian Oceans began along the Eurasian continental margin and moved the drifting Gondwanan blocks towards the Eurasian continent because of northward oceanic subduction. There may have been a unique feature during the creation of the southern Eurasian passive margin. The rifting process created several faults along the continental margin, which may serve as weak zones for future subduction. Central Iran was located upon a mantle convection cell defined by the sinking of the Paleo-Tethyan slab in the north and the upwelling of mantle in the Neo-Tethyan ridge in the south, during the interval between the Neo-Tethys opening and the Paleo-Tethyan closing.

According to subduction-driven plate tectonics of Forsyth and Uyeda (1975), the convection cell was driven by the downgoing Paleo-Tethyan oceanic slab and should continue to function even after the Paleo-Tethyan oceanic slab split from Central Iran (Conrad and Lithgow-Bertelloni, 2002). Taken together, the normal convergent force (3-5 × 10^{12} N/m) at the abrupt continent-oceanic boundary via pre-existing faults and a continuing northward mantle movement beneath the continent are likely the reasons for the subduction to begin along the southern Eurasian margin following continental collision (Fig. 6b).

Many researchers proposed that the whole-mantle convection that is bounded by upwelling of mantle plumes beneath Gondwana and downwelling beneath Eurasia may have played important roles for the Tethyan evolution (e.g. Becker and Faccenna, 2011; Jolivet et al., 2016; Faccenna et al., 2021). In our studies, we proposed that the subduction beneath Eurasia could cause continental rifting from Gondwana (Wan et al., 2021), drive continental northward drifting and trigger subduction initiation along the southern Eurasian margin. The major difference between the whole-mantle convention model and the subduction-driven model is that the upwelling of mantle plumes plays an active role in the long-lived single-directed Tethyan evolution or it is only a passive feedback of the slab subduction towards Eurasia (Chen et al., 2020). To gain deep insight into this issue demands more whole-mantle scale studies and more geological cases in the earlier history than Paleo-Tethys (Coltice et al., 2019; Robert et al., 2020; Wu et al., 2020).

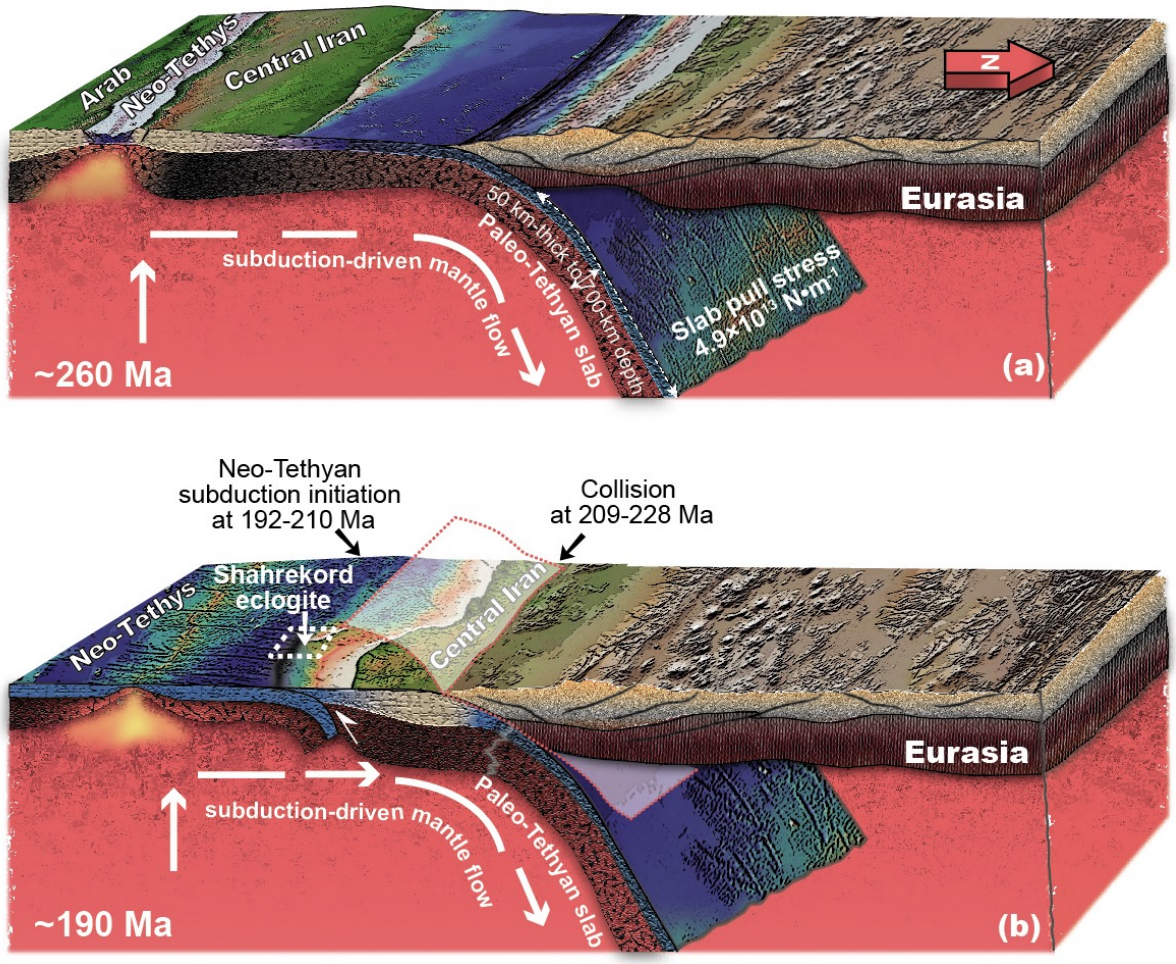

Figure 6. (a) Paleo-Tethyan subduction leads rifting to open Neo-Tethys in Iran, revised from Wan et al. (2021), (b) Collision induced Neo-Tethyan subduction initiation along the passive margin of central Iran.

5. Conclusions

- At 190 ± 11 Ma (1σ) from rutile U-Pb dates, a prograde-E-MORB-like eclogite along the Neo-Tethyan suture reached peak metamorphic condition of 2.2 GPa and 560°C. This age represents the youngest (latest) age for subduction initiation of Neo-Tethys.
- Based on regional geological events and numerical modeling results, the oldest Neo-Tethyan subduction initiation date is 192–210 Ma, which is slightly younger

than the Paleo-Tethyan closure timing of 209–228 Ma, implying collision-induced subduction initiation.

- During the rifting of Neo-Tethys, the southern margin of Central Iran inherited pre-existing faults. At such a boundary, the collision-induced force, combined with subduction-driving mantle flow, may aid in the initiation of northward subduction.

Acknowledgement

We thank Dr. Elizabeth J. Catlos for the invitation for this contribution. We appreciate the logistical help from colleagues at GSI during the fieldwork in Iran. We thank Dr. Wang, JM and Chen, Y for the P-T reconstructions. Discussions with Lin, W., Wu, FY., and Xiao, WJ. help to improve our interpretations. We thank R. Hansman for improving our writing. Comments from three anonymous reviewers and Dr. Jamshid Hassanzadeh clarify our original idea. This study was supported by the NSFC grants (91855207, 41888101).

References

Agard, P., J. Omrani, L. Jolivet, H. Whitechurch, B. Vrielynck, W. Spakman, P. Monie, B. Meyer, and R. Wortel (2011), Zagros orogeny: a subduction-dominated process, *Geological Magazine*, *148*(5-6), 692-725, doi:10.1017/S001675681100046x.

Agard, P., P. Yamato, L. Jolivet, and E. Burov (2009), Exhumation of oceanic blueschists and eclogites in subduction zones: Timing and mechanisms, *Earth-Sci. Rev.*, *92*(1–2), 53-79, doi:10.1016/j.earscirev.2008.11.002.

Ahadnejad, V., M.-V. Valizadeh, R. Deevsalar, and M. Rezaei-Kahkhaei (2011), Age and geotectonic position of the Malayer granitoids: Implication for plutonism in the Sanandaj-Sirjan Zone, W Iran, *Neues Jahrbuch für Geologie und Paläontologie-Abhandlungen*, *261*(1), 61-75.

444 Ao, S. J., W. J. Xiao, M. K. Jafari, M. Talebian, L. Chen, B. Wan, W. Q. Ji, and Z. Y. Zhang (2016), U-
445 Pb zircon ages, field geology and geochemistry of the Kermanshah ophiolite (Iran): From
446 continental rifting at 79 Ma to oceanic core complex at ca. 36 Ma in the southern Neo-Tethys,
447 *Gondwana Research*, *31*, 305-318, doi:10.1016/j.gr.2015.01.014.
448 Arvin, M., Y. Pan, S. Dargahi, A. Malekizadeh, and A. Babaei (2007), Petrochemistry of the Siah-Kuh
449 granitoid stock southwest of Kerman, Iran: Implications for initiation of Neotethys subduction,
450 *Journal of Asian Earth Sciences*, *30*(3-4), 474-489.
451 Azizi, H., and R. J. Stern (2019), Jurassic igneous rocks of the central Sanandaj–Sirjan zone (Iran)
452 mark a propagating continental rift, not a magmatic arc, *Terra Nova*, *31*(5), 415-423,
453 doi:10.1111/ter.12404.
454 Becker, T. W., and C. Faccenna (2011), Mantle conveyor beneath the Tethyan collisional belt, *Earth*
455 *and Planetary Science Letters*, *310*(3-4), 453-461, doi:10.1016/j.epsl.2011.08.021.
456 Bergman, S. C., J. S. Eldrett, and D. Minisini (2021), Phanerozoic Large Igneous Province, Petroleum
457 System, and Source Rock Links, in *Large Igneous Provinces*, edited, pp. 191-228,
458 doi:10.1002/9781119507444.ch9.
459 Bonnet, G., P. Agard, H. Whitechurch, M. Fournier, S. Angiboust, B. Caron, and J. Omrani (2020),
460 Fossil seamount in southeast Zagros records intraoceanic arc to back-arc transition: New
461 constraints for the evolution of the Neotethys, *Gondwana Research*, *81*, 423-444,
462 doi:10.1016/j.gr.2019.10.019.
463 Brown, D., and P. D. Ryan (2011), *Arc-continent collision*, 493 pp., Springer Science & Business
464 Media, Springer Heidelberg Dordrecht London New York.
465 Chen, L., X. Wang, X. Liang, B. Wan, and L. Liu (2020), Subduction tectonics vs. Plume tectonics—
466 Discussion on driving forces for plate motion, *Science China Earth Sciences*, *63*(3), 315-328,
467 doi:10.1007/s11430-019-9538-2.
468 Cherniak, D. J. (2000), Pb diffusion in rutile, *Contributions to Mineralogy and Petrology*, *139*(2), 198-
469 207, doi:10.1007/PL00007671.
470 Chiu, H.-Y., S.-L. Chung, M. H. Zarrinkoub, R. Melkonyan, K.-N. Pang, H.-Y. Lee, K.-L. Wang, S. S.
471 Mohammadi, and M. M. Khatib (2017), Zircon Hf isotopic constraints on magmatic and tectonic
472 evolution in Iran: Implications for crustal growth in the Tethyan orogenic belt, *Journal of Asian*
473 *Earth Sciences*, *145*, 652-669, doi:10.1016/j.jseaes.2017.06.011.
474 Chiu, H.-Y., S.-L. Chung, M. H. Zarrinkoub, S. S. Mohammadi, M. M. Khatib, and Y. Iizuka (2013),
475 Zircon U–Pb age constraints from Iran on the magmatic evolution related to Neotethyan
476 subduction and Zagros orogeny, *Lithos*, *162–163*, 70-87, doi:10.1016/j.lithos.2013.01.006.

Chu, Y., B. Wan, M. B. Allen, L. Chen, W. Lin, M. Talebian, and G. Xin (2021), Detrital zircon age constraints on the evolution of Paleo-Tethys in NE Iran: implications for subduction and collision tectonics, *Tectonics*, *40*, e2020TC006680, doi:10.1029/2020TC006680.

Coltice, N., L. Husson, C. Faccenna, and M. Arnould (2019), What drives tectonic plates?, *Science Advances*, *5*(10), eaax4295, doi:10.1126/sciadv.aax4295.

Conrad, C. P., and C. Lithgow-Bertelloni (2002), How mantle slabs drive plate tectonics, *Science*, *298*(5591), 207-209, doi:10.1126/science.1074161.

Coulthard Jr, D. A., M. K. Reagan, K. Shimizu, I. N. Bindeman, M. Brounce, R. R. Almeev, J. Ryan, T. Chapman, J. Shervais, and J. A. Pearce (2021), Magma Source Evolution Following Subduction Initiation: Evidence From the Element Concentrations, Stable Isotope Ratios, and Water Contents of Volcanic Glasses From the Bonin Forearc (IODP Expedition 352), *Geochemistry, Geophysics, Geosystems*, *22*(1), doi:10.1029/2020gc009054.

Davoudian, A. R., J. Genser, F. Neubauer, and N. Shabanian (2016), 40Ar/39Ar mineral ages of eclogites from North Shahrekord in the Sanandaj–Sirjan Zone, Iran: Implications for the tectonic evolution of Zagros orogen, *Gondwana Research*, *37*, 216-240, doi:10.1016/j.gr.2016.05.013.

DeMets, C., R. G. Gordon, and D. F. Argus (2010), Geologically current plate motions, *Geophysical Journal International*, *181*(1), 1-80, doi:10.1111/j.1365-246X.2009.04491.x.

Emami, N., and M. Khalili (2008), Mineralogical and geochemical constraints of Jurassic fossil hydrothermal alteration associated with an calc-alkaline volcano-sedimentary complex in Sanandaj-Sirjan Zone, Southwest of Iran, *Journal of Applied Sciences*, *8*(9), 1600-1611.

Esna-Ashari, A., M. Tiepolo, and J. Hassanzadeh (2016), On the occurrence and implications of Jurassic primary continental boninite-like melts in the Zagros orogen, *Lithos*, *258-259*, 37-57, doi:10.1016/j.lithos.2016.04.017.

Faccenna, C., T. W. Becker, A. F. Holt, and J. P. Brun (2021), Mountain building, mantle convection, and supercontinents: revisited, *Earth and Planetary Science Letters*, *564*, doi:10.1016/j.epsl.2021.116905.

Forsyth, D., and S. Uyeda (1975), On the relative importance of the driving forces of plate motion, *Geophysical Journal International*, *43*(1), 163-200.

Fürsich, F. T., M. Wilmsen, K. Seyed-Emami, M. R. Majidifard, M.-F. Brunet, M. Wilmsen, and J. W. Granath (2009), Lithostratigraphy of the Upper Triassic–Middle Jurassic Shemshak Group of Northern Iran, in *South Caspian to Central Iran Basins*, edited, pp. 129-160, Geological Society of London, doi:10.1144/sp312.6.

509 Gerya, T. V., R. J. Stern, M. Baes, S. V. Sobolev, and S. A. Whattam (2015), Plate tectonics on the
510 Earth triggered by plume-induced subduction initiation, *Nature*, *527*(7577), 221-225,
511 doi:10.1038/nature15752.
512 Guilmette, C., M. A. Smit, D. J. J. van Hinsbergen, D. Gürer, F. Corfu, B. Charette, M. Maffione, O.
513 Rabeau, and D. Savard (2018), Forced subduction initiation recorded in the sole and crust of the
514 Semail Ophiolite of Oman, *Nature Geoscience*, *11*(9), 688-695, doi:10.1038/s41561-018-0209-2.
515 Hall, R. (2017), Southeast Asia: new views of the geology of the Malay archipelago, *Annual Review of*
516 *Earth and Planetary Sciences*, *45*(1), 331-358, doi:10.1146/annurev-earth-063016-020633.
517 Hassanzadeh, J., and B. P. Wernicke (2016), The Neotethyan Sanandaj-Sirjan zone of Iran as an
518 archetype for passive margin-arc transitions, *Tectonics*, *35*(3), 586-621,
519 doi:10.1002/2015tc003926.
520 Jamali Ashtiani, R., J. Hassanzadeh, A. K. Schmitt, M. Sudo, M. Timmerman, C. Günter, and E. Sobel
521 (2020), Geochronology and geochemistry of subducted Cadomian continental basement in central
522 Iran: Decompressional anatexis along the Jurassic Neotethys margin, *Gondwana Research*, *82*,
523 354-366, doi:10.1016/j.gr.2020.01.005.
524 Jolivet, L., C. Faccenna, P. Agard, D. Frizon de Lamotte, A. Menant, P. Sternai, F. Guillocheau, and
525 A. Polat (2016), Neo-Tethys geodynamics and mantle convection: from extension to compression
526 in Africa and a conceptual model for obduction, *Canadian Journal of Earth Sciences*, *53*(11), 1190-
527 1204, doi:10.1139/cjes-2015-0118.
528 Koop, W., R. Stoneley, M. Ridd, R. Murphy, M. Osmaston, and M. Kholief (1982), Subsidence history
529 of the middle east Zagros Basin, Permian to recent, *Philosophical Transactions of The Royal*
530 *Society A: Mathematical, Physical and Engineering Sciences*, *305*, 149-167,
531 doi:10.1098/rsta.1982.0031.
532 Lawver, L. A., I. W. Dalziel, I. O. Norton, L. Gahagan, and J. Davis (2015), The PLATES 2014 Atlas of
533 Plate Reconstructions (550 Ma to Present Day), PLATES Progress Report No. 374-0215,
534 *University of Texas Institute for Geophysics Technical Reports*, 220.
535 Leng, W., and M. Gurnis (2015), Subduction initiation at relic arcs, *Geophysical Research Letters*,
536 *42*(17), 7014-7021.
537 Leven, E. J., and M. N. Gorgij (2011), Fusulinids and stratigraphy of the Carboniferous and Permian
538 in Iran, *Stratigr. Geol. Correl.*, *19*(7), 687-776, doi:10.1134/s0869593811070021.
539 Malek-Mahmoudi, F., A. Reza Davoudian, N. Shabanian, H. Azizi, Y. Asahara, F. Neubauer, and Y.
540 Dong (2017), Geochemistry of metabasites from the North Shahrekord metamorphic complex,

Sanandaj-Sirjan Zone: Geodynamic implications for the Pan-African basement in Iran, *Precambrian Research*, *293*, 56-72, doi:10.1016/j.precamres.2017.03.003.

Maunder, B., J. Prytulak, S. Goes, and M. Reagan (2020), Rapid subduction initiation and magmatism in the Western Pacific driven by internal vertical forces, *Nature communications*, *11*(1), 1874, doi:10.1038/s41467-020-15737-4.

McQuarrie, N., and D. J. J. van Hinsbergen (2013), Retrodeforming the Arabia-Eurasia collision zone: Age of collision versus magnitude of continental subduction, *Geology*, *41*(3), 315-318, doi:10.1130/G33591.1.

Merdith, A. S., S. E. Williams, S. Brune, A. S. Collins, and R. D. Müller (2019), Rift and plate boundary evolution across two supercontinent cycles, *Global and Planetary Change*, *173*, 1-14, doi:10.1016/j.gloplacha.2018.11.006.

Moghadam, H. S., Q.-L. Li, W. L. Griffin, R. J. Stern, J. F. Santos, M. N. Ducea, C. J. Ottley, O. Karsli, F. Sepidbar, and S. Y. O'Reilly (2022), Temporal changes in subduction- to collision-related magmatism in the Neotethyan orogen: The Southeast Iran example, *Earth-Sci. Rev.*, *226*, 103930, doi:10.1016/j.earscirev.2022.103930.

Moghadam, H. S., and R. J. Stern (2011), Geodynamic evolution of Upper Cretaceous Zagros ophiolites: formation of oceanic lithosphere above a nascent subduction zone, *Geological Magazine*, *148*(5-6), 762-801.

Moghadam, H. S., and R. J. Stern (2015), Ophiolites of Iran: Keys to understanding the tectonic evolution of SW Asia: (II) Mesozoic ophiolites, *Journal of Asian Earth Sciences*, *100*(0), 31-59, doi:10.1016/j.jseaes.2014.12.016.

Natal'in, B. A., and A. M. C. Şengör (2005), Late Palaeozoic to Triassic evolution of the Turan and Scythian platforms: The pre-history of the Palaeo-Tethyan closure, *Tectonophysics*, *404*(3), 175-202, doi:10.1016/j.tecto.2005.04.011.

Nikolaeva, K., T. V. Gerya, and F. O. Marques (2010), Subduction initiation at passive margins: Numerical modeling, *Journal of Geophysical Research*, *115*(B3), 10.1029/2009JB006549, doi:10.1029/2009jb006549.

Niu, Y., M. J. O'Hara, and J. A. Pearce (2003), Initiation of subduction zones as a consequence of lateral compositional buoyancy contrast within the lithosphere: a petrological perspective, *Journal of Petrology*, *44*(5), 851-866, doi:10.1093/petrology/44.5.851.

Okay, A. I., G. Sunal, S. Sherlock, A. R. C. Kylander‐Clark, and E. Özcan (2020), İzmir‐Ankara Suture as a Triassic to Cretaceous Plate Boundary—Data From Central Anatolia, *Tectonics*, *39*(5), doi:10.1029/2019tc005849.

574 Omrani, J., P. Agard, H. Whitechurch, M. Benoit, G. Prouteau, and L. Jolivet (2008), Arc-magmatism
575 and subduction history beneath the Zagros Mountains, Iran: A new report of adakites and
576 geodynamic consequences, *Lithos*, *106*(3–4), 380-398, doi:10.1016/j.lithos.2008.09.008.
577 Robert, B., M. Domeier, and J. Jakob (2020), Iapetan Oceans: An analog of Tethys?, *Geology*, *48*(9),
578 929-933, doi:10.1130/g47513.1.
579 Schellart, W. (2004), Quantifying the net slab pull force as a driving mechanism for plate tectonics,
580 *Geophysical Research Letters*, *31*(7), doi:10.1029/2004gl019528.
581 Scotese, C. R., H. Song, B. J. W. Mills, and D. G. van der Meer (2021), Phanerozoic
582 paleotemperatures: The earth's changing climate during the last 540 million years, *Earth-Sci. Rev.*,
583 *215*, doi:10.1016/j.earscirev.2021.103503.
584 Stampfli, G. M., C. Hochard, C. Vérard, C. Wilhem, and J. vonRaumer (2013), The formation of
585 Pangea, *Tectonophysics*, *593*, 1-19, doi:10.1016/j.tecto.2013.02.037.
586 Stern, R. J. (2004), Subduction initiation: spontaneous and induced, *Earth and Planetary Science*
587 *Letters*, *226*(3-4), 275-292, doi:10.1016/j.epsl.2004.08.007.
588 Stern, R. J., and T. Gerya (2018), Subduction initiation in nature and models: A review,
589 *Tectonophysics*, *746*, 173-198, doi:10.1016/j.tecto.2017.10.014.
590 Stern, R. J., H. S. Moghadam, M. Pirouz, and W. Mooney (2021), The Geodynamic Evolution of Iran,
591 *Annual Review of Earth and Planetary Sciences*, *49*(1), 9-36, doi:10.1146/annurev-earth-071620-
592 052109.
593 Sun, S. S., and W. F. McDonough (1989), Chemical and isotopic systematics of ocean basins:
594 implications for mantle composition and processes, *Geological Society of London, Special*
595 *Publications*, *42*, 313-345.
596 Syracuse, E. M., and G. A. Abers (2006), Global compilation of variations in slab depth beneath arc
597 volcanoes and implications, *Geochemistry, Geophysics, Geosystems*, *7*(5),
598 doi:10.1029/2005GC001045.
599 Topuz, G. I., G. Göçmengil, Y. Rolland, Ö. F. Çáelik, T. Zack, and A. K. Schmitt (2013), Jurassic
600 accretionary complex and ophiolite from northeast Turkey: No evidence for the Cimmerian
601 continental ribbon, *Geology*, *41*(2), 255-258, doi:10.1130/g33577.1.
602 Torsvik, T. H., and L. R. M. Cocks (2017), *Earth history and palaeogeography*, 317 pp., Cambridge
603 University Press, United Kingdom, doi:10.1017/9781316225523.
604 van Hinsbergen, D. J. J., et al. (2021), A record of plume-induced plate rotation triggering subduction
605 initiation, *Nature Geoscience*, *14*(8), 626-630, doi:10.1038/s41561-021-00780-7.

606 van Hunen, J., and M. B. Allen (2011), Continental collision and slab break-off: A comparison of 3-D
607 numerical models with observations, *Earth and Planetary Science Letters*, *302*(1), 27-37.
608 Verdel, C., B. P. Wernicke, J. Hassanzadeh, and B. Guest (2011), A Paleogene extensional arc flare-
609 up in Iran, *Tectonics*, *30*(3), doi:10.1029/2010tc002809.
610 Wakabayashi, J. (2011), Mélanges of the Franciscan Complex, California: Diverse structural settings,
611 evidence for sedimentary mixing, and their connection to subduction processes, *Geological society*
612 *of America bulletin Speical Papers*, *480*, 117-141, doi:10.1130/2011.2480(05.
613 Wan, B., Y. Chu, L. Chen, X. Liang, Z. Zhang, S. Ao, and M. Talebian (2021), Paleo-Tethys
614 subduction induced slab-drag opening the Neo-Tethys: Evidence from an Iranian segment of
615 Gondwana, *Earth-Sci. Rev.*, 103788, doi:10.1016/j.earscirev.2021.103788.
616 Wan, B., F. Wu, L. Chen, L. Zhao, X. Liang, W. Xiao, and R. Zhu (2019), Cyclical one-way continental
617 rupture-drift in the Tethyan evolution: Subduction-driven plate tectonics, *Science China Earth*
618 *Sciences*, *62*, 2005-2016, doi:10.1007/s11430-019-9393-4.
619 Wang, J.-M., P. Lanari, F.-Y. Wu, J.-J. Zhang, G. P. Khanal, and L. Yang (2021), First evidence of
620 eclogites overprinted by ultrahigh temperature metamorphism in Everest East, Himalaya:
621 Implications for collisional tectonics on early Earth, *Earth and Planetary Science Letters*, *558*,
622 doi:10.1016/j.epsl.2021.116760.
623 Whattam, S. A., and R. J. Stern (2011), The 'subduction initiation rule': a key for linking ophiolites,
624 intra-oceanic forearcs, and subduction initiation, *Contributions to Mineralogy and Petrology*,
625 *162*(5), 1031-1045, doi:10.1007/s00410-011-0638-z.
626 Whittaker, J. M., S. E. Williams, and R. D. Müller (2013), Revised tectonic evolution of the Eastern
627 Indian Ocean, *Geochemistry, Geophysics, Geosystems*, *14*(6), 1891-1909,
628 doi:10.1002/ggge.20120.
629 Williams, S. E., J. M. Whittaker, J. A. Halpin, and R. D. Müller (2019), Australian-Antarctic breakup
630 and seafloor spreading: Balancing geological and geophysical constraints, *Earth-Sci. Rev.*, *188*,
631 41-58, doi:10.1016/j.earscirev.2018.10.011.
632 Wu, F. Y., B. Wan, L. Zhao, W. J. Xiao, and R. X. Zhu (2020), Tethyan geodynamics, *Acta*
633 *Petrologica Sinica*, *36*(6), 1627-1674 (in Chinese with English abstract), doi:10.18654/1000-
634 0569/2020.06.01.
635 Yan, Z., L. Chen, X. Xiong, B. Wan, and H. Xu (2021), Oceanic plateau and subduction zone jump:
636 two‐dimensional thermo‐mechanical modeling, *Journal of Geophysical Research: Solid Earth*,
637 *126*(7), doi:10.1029/2021jb021855.

638 Zanchetta, S., F. Berra, A. Zanchi, M. Bergomi, M. Caridroit, A. Nicora, and G. Heidarzadeh (2013),
639 The record of the Late Palaeozoic active margin of the Palaeotethys in NE Iran: Constraints on the
640 Cimmerian orogeny, *Gondwana Research*, *24*(3), 1237-1266, doi:10.1016/j.gr.2013.02.013.
641 Zhang, Z., et al. (2018), Geochemistry, zircon U-Pb and Hf isotope for granitoids, NW Sanandaj-Sirjan
642 zone, Iran: Implications for Mesozoic-Cenozoic episodic magmatism during Neo-Tethyan
643 lithospheric subduction, *Gondwana Research*, *62*, 227-245, doi:10.1016/j.gr.2018.04.002.
644 Zhang, Z., W. Xiao, M. R. Majidifard, R. Zhu, B. Wan, S. Ao, L. Chen, M. Rezaeian, and R. Esmaeili
645 (2017), Detrital zircon provenance analysis in the Zagros Orogen, SW Iran: implications for the
646 amalgamation history of the Neo-Tethys, *International Journal of Earth Sciences*, *106*(4), 1223-
647 1238, doi:10.1007/s00531-016-1314-3.
648 Zhong, X., and Z.-H. Li (2020), Subduction initiation during collision-induced subduction transference:
649 numerical modeling and implications for the Tethyan evolution, *Journal of Geophysical Research:*
650 *Solid Earth*, *125*(2), e2019JB019288, doi:10.1029/2019jb019288.
651 Zhong, X., and Z.-H. Li (2022), Wedge-Shaped Southern Indian Continental Margin Without Proper
652 Weakness Hinders Subduction Initiation, *Geochemistry, Geophysics, Geosystems*, *23*(2),
653 e2021GC009998, doi:10.1029/2021GC009998.
654 Zhou, X., Z. H. Li, T. V. Gerya, and R. J. Stern (2020), Lateral propagation-induced subduction
655 initiation at passive continental margins controlled by preexisting lithospheric weakness, *Sci Adv*,
656 *6*(10), eaaz1048, doi:10.1126/sciadv.aaz1048.
657